The greenhouse effect and carbon dioxide

Wenyi Zhong and Joanna D. Haigh
Department of Physics and Grantham Institute for Climate Change, Imperial College London

Weather – April 2013, Vol. 68, No. 4

Introduction

It is well known that carbon dioxide plays an important role in the natural greenhouse warming of the Earth's atmosphere but the extent to which increases in its concentration might enhance the warming has, over the years, been controversial. The idea of climate warming related to CO_2 increases, as propounded by Arrhenius among others in the late nineteenth century, was challenged by various scientists in the early twentieth century, including Ångström who argued that the overlap of the CO_2 spectral bands with those of water vapour, combined with the saturation of absorption near the centre of the 15μm band, would leave little scope for additional effects. In the 1930s and 1940s Guy Stewart Callendar at Imperial College (London) revived the warming theory and by the 1970s it was generally accepted that global surface temperatures would increase as CO_2 concentrations increased. The band-filling and overlap effects meant the increase would not, however, be in direct proportion to CO_2 but would rather vary with the logarithm of its concentration. (For good reviews of the history of this discussion, see Mudge (1997) and, in much more detail, Weart (2008 and website update 2011)).

More recently the saturation issue has been resurrected in attempts to deny the existence of anthropogenic climate change. Very clear explanations (e.g. by Archer, 2007; Pierrehumbert, 2011) have been given of the basic physics as to why these arguments are flawed. Here we show in detail how, although the very centre of the 15μm band does become saturated, greenhouse trapping by CO_2 at other wavelengths is far from saturation and that, as its concentration exceeds approximately 800ppmv[1], its effect actually increases at a rate faster than logarithmic.

Earth's radiation budget and the Greenhouse Effect

The Earth is bathed in radiation from the Sun, which warms the planet and provides all the energy driving the climate system. Some of the solar (shortwave) radiation is reflected back to space by clouds and bright surfaces but much reaches the ground, which warms and emits heat radiation. This infrared (longwave) radiation, however, does not directly escape to space but is largely absorbed by gases and clouds in the atmosphere, which itself warms and emits heat radiation, both out to space and back to the surface. This enhances the solar warming of the Earth producing what has become known as the 'greenhouse effect'. Global radiative equilibrium is established by the adjustment of atmospheric temperatures such that the flux of heat radiation leaving the planet equals the absorbed solar flux.

The schematic in Figure 1, which is based on available observational data, illustrates the magnitude of these radiation streams. At the Earth's distance from the Sun the flux of radiant energy is about 1365Wm^{-2} which, averaged over the globe, amounts to 1365/4 = 341W for each square metre. Of this about 30% is reflected back to space (by bright surfaces such as ice, desert and cloud) leaving 0.7 × 341 = 239Wm^{-2} available to the climate system. The atmosphere is fairly transparent to short wavelength solar radiation and only 78Wm^{-2} is absorbed by it, leaving about 161Wm^{-2} being transmitted to, and absorbed by, the surface. Because of the greenhouse gases and clouds the surface is also warmed by 333Wm^{-2} of back radiation from the atmosphere. Thus the heat radiation emitted by the surface, about 396Wm^{-2}, is 157Wm^{-2} greater than the 239Wm^{-2} leaving the top of the atmosphere (equal to the solar radiation absorbed) – this is a measure of 'greenhouse trapping'.

Infrared spectral absorption by water vapour and carbon dioxide

The amount of radiation trapped depends fundamentally on the gaseous composition of the atmosphere and the spectral

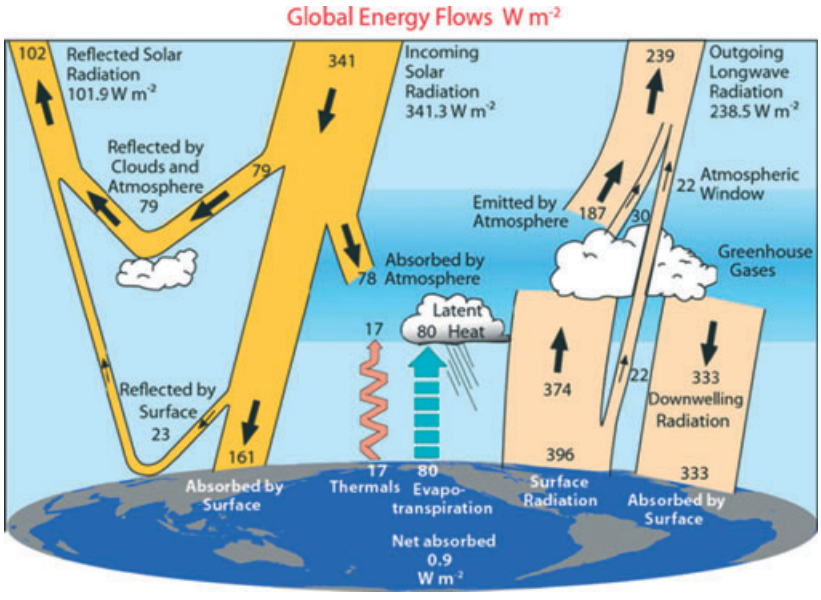

Figure 1. The global annual mean energy budget of Earth's climate system (Trenberth and Fasullo, 2012.)

[1]1ppmv indicates one molecule of the gas for every million molecules of air.

RMetS Royal Meteorological Society

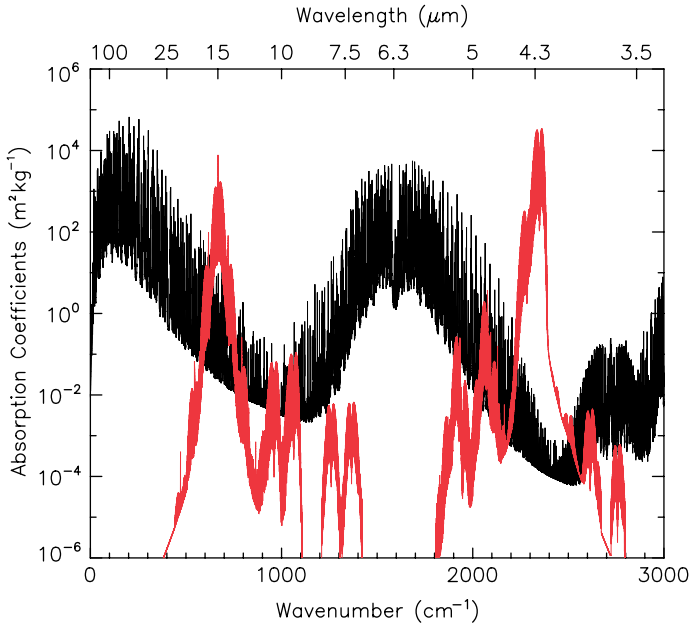

Figure 2. Absorption coefficients calculated using a line-by-line radiative transfer model (Francis and Edwards, 2007) with the HITRAN2004 spectral database for water vapour (black curve) and carbon dioxide (red curve) as function of wavenumber/wavelength. The horizontal scale is linear in wavenumber (cm^{-1}, on bottom axis) because this produces a plot in which area is proportional to the flux of energy. The equivalent wavelength is presented on the top axis. HITRAN (High-resolution transmission molecular absorption) is a spectroscopic database widely used to predict and simulate the transmission and emission of radiation in the atmosphere. This long-term project was started in the 1960s by Air Force Cambridge Research Laboratories (AFCRL) and is updated regularly. The latest version, HITRAN2008 (Rothman et al., 2009), contains 2 713 968 lines for 39 different species, among which water vapour and carbon dioxide are the ones of greatest importance.

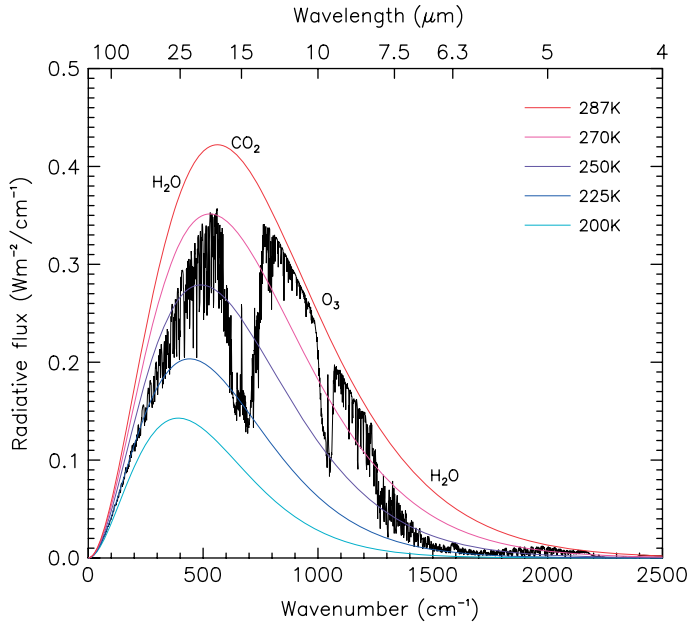

Figure 3. The black curve is a model-generated spectrum of the infrared radiative flux emitted to space at the top of the atmosphere (OLR). Coloured lines represent the blackbody spectrum at different temperatures (see legend). Regions of reduction in OLR due to the H_2O rotation bands (0–540cm^{-1}), CO_2 15μm band (550–800cm^{-1}), O_3 9.6μm band (980–1100cm^{-1}) and H_2O 6.3μm band (1400–1800cm^{-1}) are identified.

properties of the gases. The major atmospheric constituents, nitrogen and molecular oxygen, have no absorption properties at infrared wavelengths and the main greenhouse gas is water vapour, with carbon dioxide the next most important. The spectral properties of H_2O and CO_2 are portrayed in Figure 2 which presents the infrared absorption coefficients per unit mass of pure gas at a pressure of 600mbar and temperature of 250K (note that these conditions are not representative of those in the Earth's atmosphere but are used here to illustrate the spectral properties). There are two broad features of H_2O absorption centred in the far-infrared (>15μm) and around 6.3μm, leaving broad regions of lesser absorption centred near 12μm and 4μm. The CO_2 spectrum has much sharper features centred around two main bands at 15μm and 4.3μm which lie, coincidentally, in the windows of the H_2O spectrum. We note for future reference the sub-bands of CO_2 lying near 10μm.

The role of different gases in the absorption and trapping of radiation in the atmosphere is illustrated in Figure 3. This shows the spectrum of the radiative flux leaving the top of the atmosphere (TOA), calculated for a cloudless atmosphere, with global mean vertical profiles of temperature for H_2O and O_3, and the Earth's surface a black body at a temperature of 287.13K. Three other well-mixed greenhouse gases are included with concentrations for CO_2 of 389ppmv, CH_4 1.76ppmv and N_2O 0.316ppmv. Also in the figure coloured curves are shown, representing the spectra of radiation which would be emitted by black bodies at the temperatures given in the legend. The red curve is calculated at the surface temperature and if there were no atmosphere to interfere with the radiation then the emitted TOA spectrum would coincide with this. Clearly, however, the black curve falls below the red one at all wavelengths indicating that less radiation is emitted to space than leaves the surface. Dips in the curve indicate the wavelengths at which there is strong absorption by greenhouse gases of the radiation emanating from the ground and thus a greater contribution to the TOA flux from layers higher, and colder, in the atmosphere. The effective radiating temperature at each wavelength can be gauged by comparison with the blackbody curves at lower temperatures. The area under the black curve, being 257.7Wm^{-2}, represents the total flux of longwave radiative energy leaving the planet (this is not identical to the 239Wm^{-2} identified in Figure 1 because we have assumed cloud-free skies here). Spectra calculated in this way, using the correct atmospheric profiles, agree closely with satellite measurements of the infrared spectrum leaving the Earth, providing verification both for the radiative transfer theory and the spectral line database.

The black and red curves lie closely together in the spectral regions where the radiation is coming from at or near the surface. Regions of lower H_2O absorption identified in Figure 2, under conditions of high humidity, have a significant influence on longwave fluxes due to 'continuum absorption'. This is important for downward flux but, as the emission is coming from air near the surface, it is not apparent at the TOA. Large deviations between the black and red curves can be seen in the large bites around 15μm due to CO_2 and 9.6μm due to O_3. The

Weather – April 2013, Vol. 68, No. 4

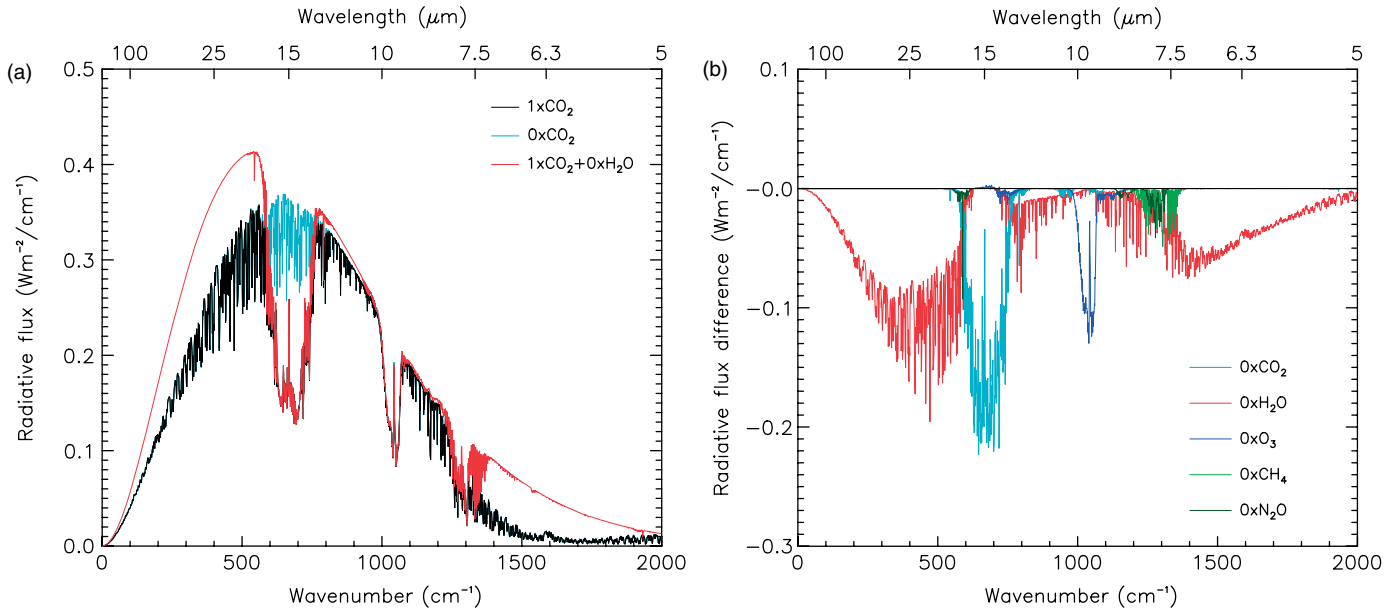

Figure 4. (a) Calculated infrared spectra of outgoing fluxes at the top of the atmosphere for a global mean atmosphere with current concentrations of water vapour, CO_2, O_3, CH_4 and N_2O (black curve); same conditions as the black but with all water vapour removed (red curve); same but with all CO_2 removed (sky blue curve). The data are plotted as a function of wavenumber (proportional to photon energy) with equivalent wavelengths being shown on the horizontal axis at the top of the plot. (b) The difference between outgoing flux at the top of the atmosphere with the current atmosphere and with gases individually removed (see legend). Negative values indicate that the presence of a gas reduces the emission of infrared radiation to space. See legend for Table 1 for the rationale behind this exercise.

CO_2 15μm absorption is particularly significant because this wavelength lies near the peak of the blackbody spectrum at the emitting temperature. The strong absorption by CO_2 at 4.3μm, as identified in Figure 2, has very little influence, however, as it lies well away from this peak.

Greenhouse trapping of infrared radiation

To investigate the greenhouse effect of different atmospheric components we calculate the TOA spectrum for cases in which each gas is removed in turn. The black curve in Figure 4(a) is the same as in Figure 3 while the red curve represents a situation with the same temperature profile, and the same concentrations of CO_2, O_3, CH_4 and N_2O, but with all the H_2O removed. This lies above the black curve at all wavelengths but especially at the extremes of the wavelength range, indicating greenhouse trapping by H_2O. The difference between the two results is presented by the red curve in Figure 4(b). The sky blue curves in Figure 4(a) and (b) show the calculation for the standard profile but with all the CO_2 removed, illustrating that CO_2 has a significant greenhouse effect despite its absorption being confined to narrow bands rather than the very broad spectral features of water vapour. This comes about because it happens that the strong CO_2 band near 15μm not only coincides with the peak of the spectrum of radiation emitted at temperatures typical of the Earth's surface but also lies in a region of relatively weak H_2O absorption. Also shown in Figure 4(b) are similar calculations carried out with ozone, methane and nitrous oxide removed. O_3 has an absorption band around 9.6μm, CH_4 and N_2O weaker ones around 8μm and 17μm. Integrated over the entire spectrum, the areas under the curves in Figure 4(b) indicate the greenhouse trapping by each of the gases and thus provide an indication of the roles they play in warming the surface of the planet.

Table 1 presents the contributions of the individual gases (derived from the areas under the curves in Figure 4(b)). The second row in the table shows the impact of the individual gases on downward radiation incident at the surface. This component is dominated by H_2O due to the very strong emission of radiation by the near-surface atmosphere through the H_2O continuum described above. At the top of the atmosphere, however, the continuum has little effect as most of the radiation emitted by H_2O in lower layers has been absorbed and the emergent radiation has been emitted from layers at lower temperatures. For CO_2, on the other hand, some of the radiation from the surface manages to reach space. Thus the net effects of H_2O and CO_2 at the top of the atmosphere are much more similar than at the surface and it can be seen that, despite having a concentration of less than 0.04%, CO_2 is responsible for nearly a quarter of the total greenhouse trapping of radiation in the current atmosphere under clear-sky conditions.

Also shown in Table 1 is the increase in net (downward minus upward) radiative flux at the tropopause. The magnitudes of these are similar to the TOA values with the differences determined by the effect of the stratosphere on downward fluxes at the tropopause and upward fluxes at the TOA. The amount of energy trapped in the troposphere-surface system determines the

Table 1

The impact on infrared radiative fluxes (Wm^{-2}) of the presence of the atmosphere and of individual gases within it, calculated from the difference between an atmosphere with all gases and that with the named gas removed.

	H_2O	CO_2	O_3	CH_4	N_2O
Outgoing flux at TOA	−70.6	−25.5	−7.0	−1.7	−1.8
Downward flux at the surface	208.0	16.0	2.6	0.8	0.8
Net (downward – upward) flux change at the tropopause	77.3	38.2	4.3	1.7	2.6

The estimates are done in this way because the overlapping of the wavelength regions in which absorption occurs means that the impact of any particular gas is sensitive to the presence of other gases. Calculating the effect of a gas in isolation thus overestimates its impact.

so-called radiative forcing of climate, discussed later.

Saturation of carbon dioxide absorption

We now look in more detail at the role of carbon dioxide in determining atmospheric radiative fluxes and at how this may change as its concentration continues to rise. Figure 5(a) presents TOA spectra with current atmospheric conditions but using five different CO_2 concentrations: 0, 1.5, 389, 2 × 389 and 32 × 389 ppmv. The light blue curve represents zero CO_2 and the green curve shows that adding as little as ~1.5ppmv CO_2 in the atmosphere has a significant impact with strong absorption in the centre of the band. The black curve shows the calculated spectrum for the current concentration of CO_2 (389ppmv), with a deepening and widening of the absorption region. The differences between each spectrum and that for the current level are illustrated in Figure 5(b). The purple line shows the band widening further on a doubling of CO_2 but in the very centre of the band the flux now increases slightly. This is because the greater optical depth at band centre means that the level of the atmosphere from which most radiation reaches space has moved further up into the stratosphere, where temperatures increase with altitude (note, though, that in the stratosphere enhanced CO_2 concentrations result in lower temperatures which counteract the increased emission at band centre). For very high CO_2 concentration, the red curve shows an enhancement of these effects: the band centre produces greater emission but the band wings are absorbing more.

Another striking feature in the red spectrum is that the minor bands of CO_2 around 10μm (either side of the 9.6μm O_3 band) show a marked response. The reductions in irradiance in the wings of the 15μm band and in the 10μm bands compensate for the increases in the band centre. In the next section we consider how their net effect influences CO_2 radiative forcing of climate.

Climate radiative forcing by carbon dioxide

The radiative energy trapped by greenhouse gases is absorbed into the climate system, warming the lower atmosphere. It has been demonstrated that, to a first approximation, the global mean surface temperature changes in proportion to the trapped radiative flux, leading to the concept of the radiative forcing of climate change. A basic definition of instantaneous Radiative Forcing (RF) is the (hypothetical) change in the net downward radiative flux at the tropopause in response to any

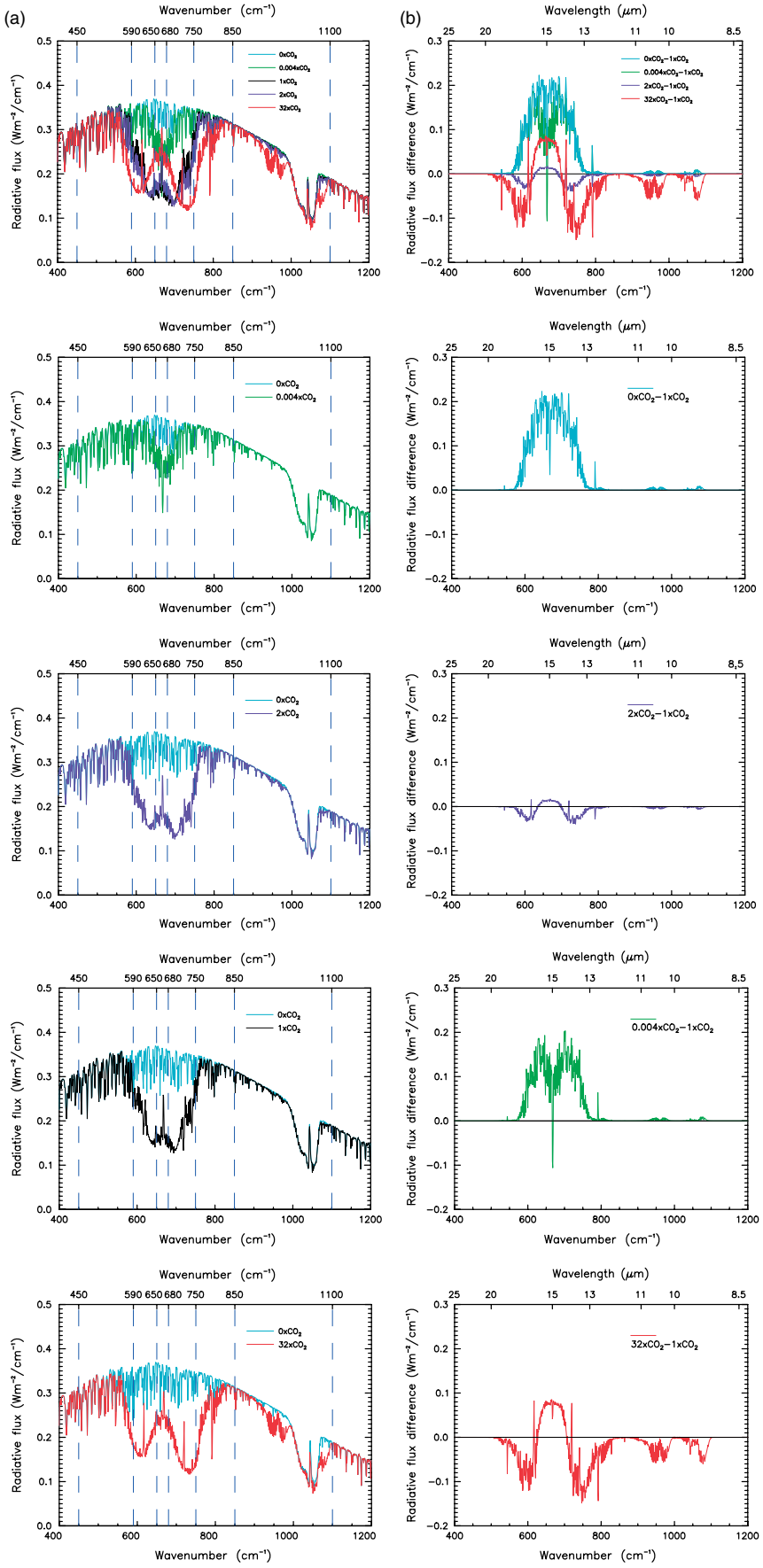

Figure 5. (a) The top of atmosphere infrared spectrum calculated with CO_2 mixing ratio (ppmv) of 0 (light blue curve), 1.5ppmv (green), 389ppmv (black), 2 × 389ppmv (purple) and 32 × 389ppmv (red). The vertical dashed lines mark the sub-intervals discussed in the text: the CO_2 15μm band core (650–680cm^{-1}), the band central regions (590–650cm^{-1} and 680–750cm^{-1}), the band wings (450–590cm^{-1}and 750–850cm^{-1}), and the CO_2 10μm bands (850–1100cm^{-1}) which overlap the O_3 9.6μm band. (b) The differences between each CO_2 spectrum in Figure 5(a) from that with the current CO_2 concentration (389ppmv).

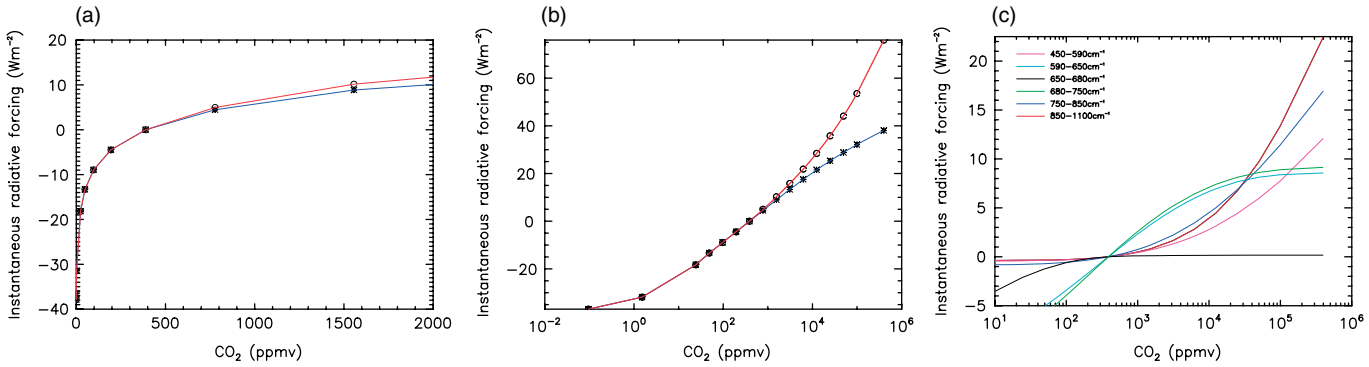

Figure 6. (a) Instantaneous Radiative Forcing of CO_2 (relative to the present-day concentration) as a function of volume mixing ratio. The red curve is for the whole infrared region, 0–3000cm^{-1}. The blue curve covers only the spectral region 550–800cm^{-1} (i.e. the 15μm band). (b) As (a) but extending to higher CO_2 mixing ratios and presented against the logarithm of volume mixing ratio. (c) Radiative Forcing against CO_2 mixing ratio for the six spectral intervals.

perturbing factor before the atmosphere has adjusted to the forcing.[2] Thus our calculations assume no change in the surface or atmosphere, do not consider the climate response to the RF, or any issues related to climate sensitivity, but focus on variations in the radiative balance introduced by varying concentrations of CO_2.

We calculate the RF of CO_2, relative to the current situation, over a wide range of concentrations using the same conditions and radiative transfer codes as outlined above. Seventeen values of CO_2 mixing ratio are used, ranging from zero to 1024 times the current value, which is an atmosphere composed of about 40% CO_2. The red curve in Figure 6(a) shows the RF values for CO_2 volume mixing ratios up to 2000ppmv. Removing all the CO_2 from the current atmosphere produces a RF of −38Wm^{-2} (as in the bottom row of Table 1). The RF increases sharply as the CO_2 concentration rises from zero. At higher concentrations the rate of increase lessens gradually, but it is always positive. Figure 6(b) extends Figure 6(a) to higher mixing ratios and with a logarithmic coordinate for mixing ratio. It can be seen that between approximately 30 and 800ppmv the RF increases linearly with log(mixing ratio), demonstrating the familiar current behaviour but that at higher concentrations it starts to increase more sharply.

To investigate this behaviour we divide the infrared spectrum in the CO_2 absorption region (450–1100cm^{-1}) into six intervals, as presented by the vertical dashed lines in Figure 5(a). These cover the CO_2 15μm band core (650–680cm^{-1}), the near-core regions (590–650cm^{-1} and 680–750cm^{-1}), the band wings (450–590cm^{-1} and 750–850cm^{-1}) and the 10μm minor bands (850–1100cm^{-1}). Figure 6(c) shows the variations of RF with CO_2 mixing ratio for each of these spectral intervals. At concentrations higher than at present the black curve is essentially horizontal, indicating that the band core is saturated. The near-core regions (green and cyan curves) show a slowing down of the increase but remain unsaturated up to at least a CO_2 mixing ratio of 10^5ppmv. The band wings (blue and pink lines) are far from saturation even when approaching a near-pure CO_2 atmosphere. The forcing due to the 10μm bands (red curve) is about 6.5% of the total RF for a doubling of CO_2 (slightly larger than the 6.1% found in the first estimate of their effect by Augustsson and Ramanathan (1977)). It has the fastest increasing rate and becomes the largest forcing at mixing ratios greater than about 3×10^4ppmv. It is the sum of these effects that produces the total behaviour shown by the red curve in Figure 6 (a) and (b). Also shown in this figure, by the blue lines, is the RF from just the 15μm region (550–800cm^{-1}) as used in many climate models. From these it can be seen that, as mixing ratios rise above values greater than approximately double the current level, the neglect by climate models of the 10μm bands would lead to increasing underestimates of CO_2 RF.

Summary

The greenhouse effect on Earth results in the mean surface temperature increasing from a value of 255K (−18°C), which it would adopt with no atmosphere under radiative equilibrium conditions, to the current observed level of 287K (+14°C). In this paper we have used calculations of the absorption and emission of infrared radiation by the atmosphere to investigate how different parts of the spectrum, and different atmospheric gases, contribute to the greenhouse effect.

The strongest water vapour absorption occurs in spectral bands at wavelengths longer than about 17μm and shorter than about 8μm. The strongest absorption bands of CO_2 are those at 15μm and 4.3μm, followed by weaker bands around 10μm. The CO_2 15μm band occurs close to the peak of the blackbody function at temperatures representative of the Earth's atmosphere and surface. It also happens to occur where water vapour absorption is weaker and thus it plays a key role in infrared radiative transfer in Earth's atmosphere. The CO_2 4.3μm absorption coefficients are the strongest in the infrared region but are located where the radiative intensity is much weaker. Thus, although it plays a role in the upper atmosphere, this band is unimportant to the greenhouse effect on Earth.

Calculations at very high spectral resolution, and using state-of-the-art data for gaseous absorption properties, indicate that as the atmospheric CO_2 concentration rises from zero the total (instantaneous) RF at first grows very sharply but the rate of increase moderates such that for concentrations between about 30 and 800ppmv RF increases in proportion to log(mixing ratio). This is the situation in the contemporary atmosphere, for which the concentration is 389ppmv and total RF about 38Wm^{-2}. For higher concentrations, however, the rate of increase becomes supra-logarithmic. This is because, while the centre of the 15μm band becomes saturated, the band wings and, especially, the 10μm bands become dominant in determining the radiative effects – and these are nowhere near saturation.

The 'adjusted' value, as used by the IPCC (e.g. 2001), takes account of the (fast) temperature response of the stratosphere to composition changes. For CO_2 the adjusted value is about 20% lower than the instantaneous value. We assume a clear sky while the inclusion of cloud in the atmosphere also reduces the RF calculated for CO_2 increases. We also neglect the small (~5%) contribution of CO_2 RF in the shortwave spectral region. Thus our absolute RF values are not directly comparable with those usually quoted for climate change. These amendments, however, have no bearing on the main emphasis of this work and our conclusions concerning the variation of CO_2 RF with mixing ratio and the importance of different parts of the infrared spectrum.

We conclude that as the concentration of CO_2 in the Earth's atmosphere continues to rise there will be no saturation in its absorption of radiation and thus there can be no complacency with regards to its potential to further warm the climate.

References

Augustsson T, Ramanathan V. 1977. A radiative-convective model study of the CO_2 climate problem. *J. Atmos. Sci.* **34**: 448–451.

Archer D. 2007. *Global Warming: Understanding the Forecast*. Blackwell Publishing Ltd.: Malden, MA.

Francis J, Edwards D. 2007. GENLN3. http://acd.ucar.edu/~edwards/ (accessed 17 December 2012).

IPCC. 2001. *Climate Change 2001 The Scientific Basis. Contribution of Working Group 1 to the Third Assessment Report of the Intergovernmental Panel on Climate Change*, Houghton JT *et al.* (eds). CUP.

Mudge FB. 1997. The development of the 'greenhouse' theory of global climate change from Victorian times. *Weather* **52**: 13–17.

Pierrehumbert RT. 2011. Infrared radiation and planetary temperature. *Phys. Today* **64**: 33–38.

Rothman LS *et al*. 2009. The HITRAN 2008 molecular spectroscopic database. *J. Quant. Spectrosc. Radiat. Transfer* **110**: 533–572.

Trenberth KE, Fasullo JT. 2012. Tracking earth's energy: from El Niño to global warming. *Surv. Geophys.* **33**: 413–426. doi:10.1007/s10712-011-9150-2

Weart SB. 2008. *The Discovery of Global Warming*. Harvard University Press and additional information at http://www.aip.org/history/climate/co2.htm (accessed 17 December 2012).

Recommended Further Reading

Kiehl JT, Trenberth KE. 1997. Earth's annual global mean energy budget. *Bull. Am. Meteorol. Soc.* **72**(2): 197–208.

Royal Society. 2010. Climate change: a summary of the science. http://royalsociety.org/policy/publications/2010/climate-change-summary-science/ (accessed 17 December 2012).

Schmidt GA *et al*. 2010. Attribution of the present-day total greenhouse effect. *J. Geophys. Res.* **115**: D20106. doi:10.1029/2010JD014287

Correspondence to: Wenyi Zhong
w.zhong@imperial.ac.uk

DOI: 10.1002/wea.2072

Weather – April 2013, Vol. 68, No. 4

The *Braer* storm revisited

Luke Odell, Peter Knippertz, Steven Pickering, Ben Parkes and Alexander Roberts

School of Earth and Environment, University of Leeds

Introduction

In a 24-hour period between 9 and 10 January 1993, a storm system in the north Atlantic (Figure 1(a)) underwent explosive cyclogenesis, deepening 78mbar and setting a record minimum central sea-level pressure of 914mbar (Figure 1(b)). The deepening over 24 hours, 3.25 Bergerons[1], is the largest on record for an extratropical cyclone (Lim and Simmonds, 2002). The storm is named after the oil tanker MV *Braer*, which was travelling from Bergen (Norway) to Quebec (Canada). On the morning of 5 January 1993 the ship lost power and began to drift helplessly in the rough seas to the north of Scotland. It later ran aground at Garths Ness, 25 miles south of Lerwick (Shetland). The ensuing storm produced gusts in excess of 100kn over Shetland, which finally broke up the MV *Braer* and released 85 000 tonnes of light crude oil into the North Sea. Fortunately no human lives were lost, but some 1500 sea birds died.

[1] One Bergeron corresponds to a fall of 24mbar in mean sea-level pressure in 24 hours at 60 °N

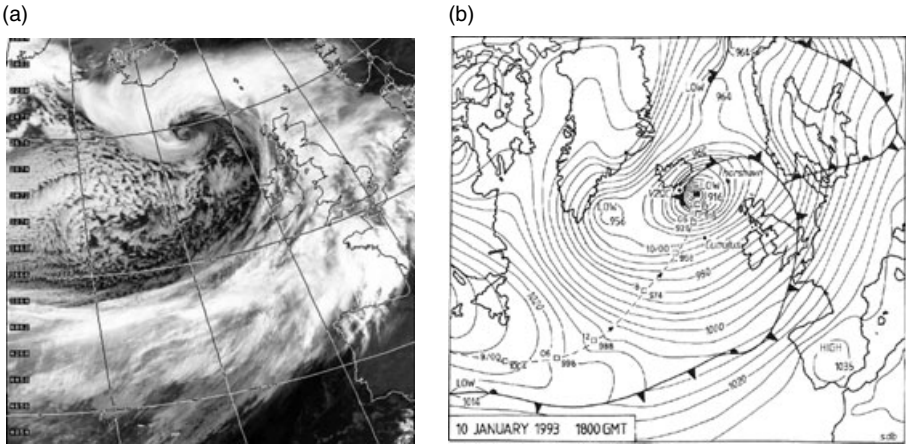

Figure 1. The Braer storm near peak strength on 10 January 1993. (a) Infrared image taken from the AVHRR satellite on a westerly pass over the UK (courtesy of www.satdundee.ac.uk) at 0920 UTC. (b) Surface analysis chart at 1800 UTC (taken from Burt (1993)).

In contrast to heavier North Sea oil, the light crude oil the MV *Braer* contained was broken up quite easily by the turbulent sea and after 21 January there was no visible oil left on the sea surface. Further impacts included blizzards in Scotland and heavy rain and gales for the rest of Britain, but the storm caused minimal other damage.

Two analyses of the *Braer* storm were published in *Weather* shortly after its occurrence (Burt, 1993; McCallum and Grahame, 1993). Both are mostly descriptive accounts of the storm, detailing observations from ships, buoys and land; an analysis of the state of the atmosphere at this time and how it conspired to produce a storm of such record-breaking intensity has remained absent from the literature. This is probably mostly the result of the lack of damage wrought, owing to the storm's track between Iceland and Scotland. The 20th anniversary of the *Braer* storm this year motivated us to revisit this highly unusual cyclone using modern reanalysis data from the European Centre for Medium-Range Weather Forecasts (ECMWF) ERA-Interim dataset, and high-resolution simulations with the Weather Research and Forecasting (WRF) model. In this article, we will focus first on the main dynamical factors contributing to the rapid deepening of the cyclone. We will then present results of sensitivity experiments to investigate the influence of orographic